

Original article

Impact of key parameters on far-field temporary plugging and diverting fracturing in fractured reservoirs: A 2D finite element study

Pingli Liu^{1,2}, Fengcheng Lou^{1,2}, Juan Du^{1,2}, Xiang Chen^{1,2*}, Jinming Liu^{1,2}, Muming Wang³

¹National Key Laboratory of Oil and Gas Reservoir Geology and Exploitation, Southwest Petroleum University, Chengdu 610500, P. R. China

²Petroleum Engineering School, Southwest Petroleum University, Chengdu 610500, P. R. China

³Department of Chemical and Petroleum Engineering, University of Calgary, Calgary T2N1N4, Canada

Keywords:

Fractured reservoir
diverting fracturing
temporary plugging
finite element method

Cited as:

Liu, P., Lou, F., Du, J., Chen, X., Liu, J., Wang, M. Impact of key parameters on far-field temporary plugging and diverting fracturing in fractured reservoirs: A 2D finite element study. *Advances in Geo-Energy Research*, 2023, 10(2): 104-116.

<https://doi.org/10.46690/ager.2023.11.05>

Abstract:

Temporary plugging and diverting fracturing technology is of utmost importance in stimulating fractured reservoirs. However, studies investigating the mechanisms of new fracture initiation and propagation during far-field temporary plugging and diverting fracturing have been scarce, and the optimal technique parameters are still unknown. To address this issue, a two-dimensional fracturing model is developed via the finite element method in this work, which simulates the temporary plugging effect using the equivalent viscosity temporary blockage method and the unrestrained growth of hydraulic fractures by globally embedding the cohesive element of zero-thickness. Then, some key parameters for far-field temporary plugging and diverting fracturing in fractured reservoirs are discussed and some interesting insights are given. Firstly, a lower-permeability plugging zone expedites the pressure increase within the fracture, thereby boosting the probability of achieving temporary plugging and diverting fracturing. The size of the plugging zone significantly impacts the pressure increase within the fracture. Secondly, the plugging position should be determined considering the density and arrangement of natural fractures in the layer, and the temporary plugging construction should be performed after maximizing the elongation of initial hydraulic fracture. Thirdly, an increase in fluid viscosity and injection displacement promotes the pressure rise inside the fracture. Nonetheless, the impact of injection displacement on temporary plugging and diverting fracturing surpasses that of fluid viscosity. Overall, the established model can inform the design of temporary plugging and diverting fracturing in fractured reservoirs.

1. Introduction

Temporary plugging and diverting fracturing (TPDF) is a crucial strategy in tight or shale reservoir stimulation. It involves the temporary positioning of materials, including fibres, particulates and gel, within the fractures or at the fracture entrances, thereby creating a temporary plugging zone (Li et al., 2018; Zhao et al., 2020). This action results in escalated pressure, subsequently initiating new fractures (Wang et al., 2020b). After fracturing treatment, the plugging material either dissolves in the working fluid or degrades under

the formation temperature and pressure, thereby minimizing reservoir damage (Zhou et al., 2022). This technique facilitates establishing a complex and high-conductivity fracture network within the reservoir, effectively boosting oil and gas production (Chen et al., 2021; Jiang and Bian, 2021).

The exploration of hydraulic fracture simulation has evolved considerably over time (Abdelaziz et al., 2023). Relevant studies initially focused on classical two-dimensional (2D) models such as the Khristianovic-Geertsma-de Klerk models (Geertsma and Haafkens, 1979). The research later

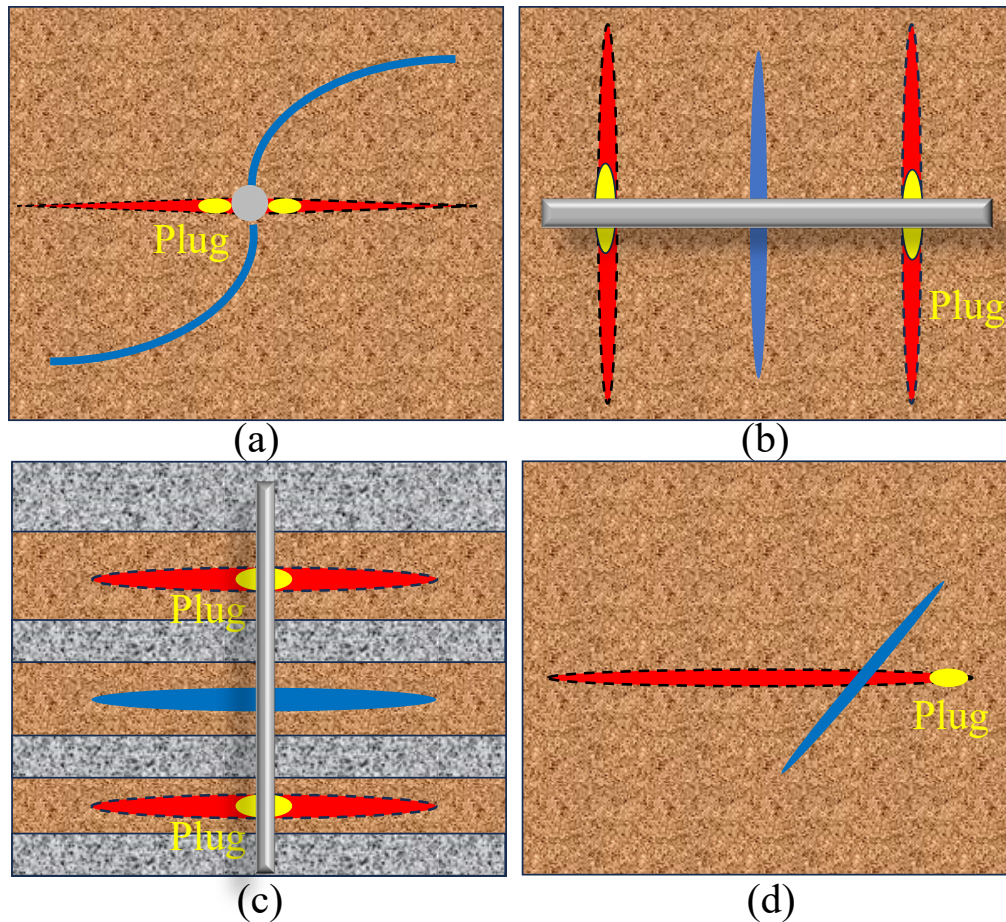


Fig. 1. Schematic diagram of TPDF. (a) Near-wellbore in-plane TPDF; (b) multi-stage TPDF in horizontal wells; (c) separate-layering TPDF; and (d) FTPDF (Wang et al., 2020a).

expanded to quasi-three-dimensional models, including the blocky and cellular models (Settari and Cleary, 1986). Eventually, fully three-dimensional (3D) models were developed, such as the moving mesh and the fixed mesh methods (Clifton and Abou, 1981). The challenge of fracture interaction prompted the creation of non-planar models, ranging from 2D (Wu and Olson, 2015, 2021; Li et al., 2020) to quasi-three-dimensional (Meyer and Bazan, 2011; Wang et al., 2020b) and 3D models (Weng et al., 2011; Kresse et al., 2012; Zhang et al., 2019). These models further investigated the patterns of fracture propagation under the influence of multiple fractures. In recent years, the simulation of TPDF fracture propagation, which constitutes a non-planar problem, has attracted the attention of many scholars (Wang et al., 2017).

Hydraulic fracture (HF) propagation in complex fractured reservoirs is influenced by comprehensive factors related to geology (e.g., natural fracture (NF) intensity and horizontal stress difference (HSD)), injection (e.g., injection displacement and fluid viscosity), and temporary plugging (e.g., characteristics, location, and timing of plugging area). Wang et al. (2020a) replaced the original elements with spring elements to construct a planar 3D model of the interaction between HF and NF. Their results indicated that factors such as NF intensity, plugging position and HSD significantly influence TPDF; smaller HSD

and intersection angles between HF and NF facilitate the creation of more complex fracture systems. Li et al. (2020) developed a 2D model for temporarily plugging staged fracturing to examine the extension mode of multi-cluster HF under temporarily plugging staged fracturing conditions. Chen et al. (2022) constructed a planar 2D model for temporary plugging fracturing in gravel reservoirs, simulated HF propagation by incorporating viscous elements and achieved plugging by increasing the dynamic fluid viscosity. Wang et al. (2022b) developed a 3D model for temporary plugging fracturing using the discrete lattice method and investigated the impact of key parameters such as injection rate and cluster spacing on the expansion of repeated fracturing of multiple fracture clusters. Relevant studies primarily concentrated on investigating the influence of geological and injection factors, failing to address the influence degree and mechanics of plugging parameters on fractured reservoir hydraulic fracture propagation.

Four typical cases of TPDF exist (Fig. 1), including near-wellbore in-plane TPDF, multi-stage TPDF in horizontal wells, separate-layering TPDF, and far-field temporary plugging and diverting fracturing (FTPDF). Most existing research focuses on the first three types, which involve temporarily plugging an existing HF at the wellbore. However, FTPDF within the fracture has received comparatively less attention, and the

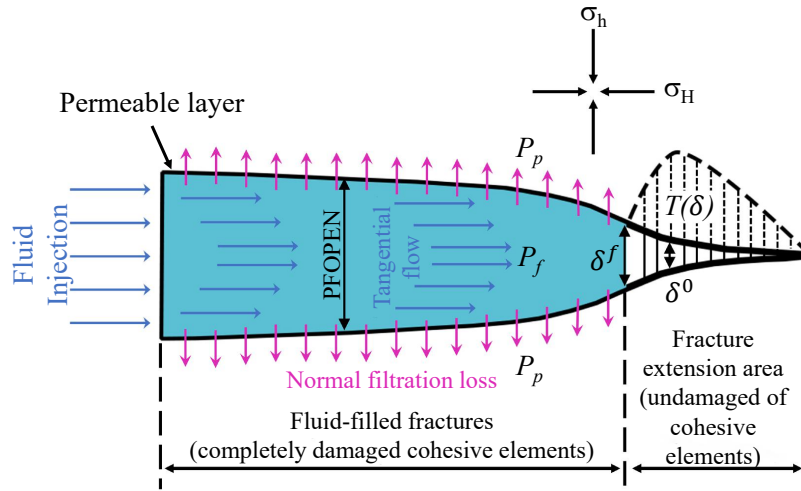


Fig. 2. Schematic tangential and normal flow diagram within a cohesive element.

mechanism of FTPDF remains ambiguous. Consequently, this paper establishes a 2D FTPDF model for a fracture-porous reservoir using the finite element method, which investigates the effects of key parameters such as permeability, length, position, and timing of the plugging area.

2. Theory and methods

2.1 Governing equations

Petroleum reservoir is a typical porous medium, and the effective stress at any point in the reservoir is (Hunt and Batchelor, 1968):

$$\bar{\sigma} = \sigma + [xp_w + (1-x)p_a]\mathbf{I} \quad (1)$$

where $\bar{\sigma}$ and σ respectively represent the effective stress and total stress tensor; p_w and p_a respectively represent the pressure of the wetted-phase fluid and other fluids in the pore space; x represents a coefficient related to saturation and interfacial tension; and \mathbf{I} represents the unit tensor. It is assumed that the water in the reservoir is saturated (i.e., $x = 1$) and the partial pressures of fluids other than water are ignored. Eq. (1) is simplified to:

$$\bar{\sigma} = \sigma + p_w\mathbf{I} \quad (2)$$

The flow is considered as Darcy flow, so the fluid percolation velocity v_w can be written as:

$$\begin{aligned} v_w &= -\frac{1}{n_w\rho_w g}k(\nabla p_w - \rho_w g) \\ &= -\frac{1}{n_w\rho_w g}\hat{K}\frac{\rho_w g}{\mu}(\nabla p_w - \rho_w g) \end{aligned} \quad (3)$$

where k represents the permeability coefficient, n_w represents the void ratio; ρ_w represents the density of the injected fluid; g represents the acceleration due to gravity; ∇p_w is the pressure gradient; \hat{K} represents the inherent permeability of the porous medium; and μ represents the fluid viscosity. While ignoring the mechanical forces, the weak form of the continuity equation in pore space can be expressed as (Wang et al., 2018):

$$\begin{aligned} \int_{\Omega} \zeta_w \frac{1}{J} \dot{p}_w d\Omega + \int_{\Omega} \zeta_w \alpha \nabla u d\Omega + \int_{\Omega} \frac{\hat{K}}{\mu} \nabla \zeta_w \nabla \dot{p}_w d\Omega \\ - \int_{\Gamma_{HF}} \zeta_w q_l d\Gamma = - \int_{\Gamma_{in}} \zeta_w \bar{q}_w d\Gamma \end{aligned} \quad (4)$$

where ζ_w represents the test function corresponding to the fluid pressure, which satisfies the uniform boundary condition; J represents the volume change of fluid in porous media; \dot{p}_w represents the fluid pore pressure's rate of change; α represents the porous elastic coefficient, also known as the Biot coefficient, which is related to rock properties; q_l represents the local fluid loss; \bar{q}_w represents the fluid outflow; Ω represents the linear elastic permeable medium domain; Γ represents the area boundary; Γ_{HF} represents the area boundary of HF; Γ_{in} represents the total area boundary; and ∇u represents the rate of change of the displacement vector.

Due to the significant difference in width compared to length and height, fractures can be modeled as an incompressible fluid with continuous flow between two flat porous plates. The flow of fluid within the fractures is categorized into tangential flow along the fracture and perpendicular normal filtration to the fracture wall (Fig. 2).

As per Poiseuille's law, the equation dictating the flow of fluids within the fracture is formulated as follows (Geertsma and Haafkens, 1979):

$$q = -\frac{w^3}{12\mu} \nabla p \quad (5)$$

where q represents the flow rate within the fracture; ∇p represents the along-range pressure drop gradient in the tangential direction of the fracture; and w represents the fracture width. Moreover, the normal flow is expressed as (Yu et al., 2019):

$$q_l = 2c(p_f - p_p) \quad (6)$$

where q_l represents the filtration rate; c represents the filtration coefficient; p_p represents the pore pressure; and p_f represents the fracture pressure. By integrating Eqs. (3) and (6), the mass conservation equation is derived as:

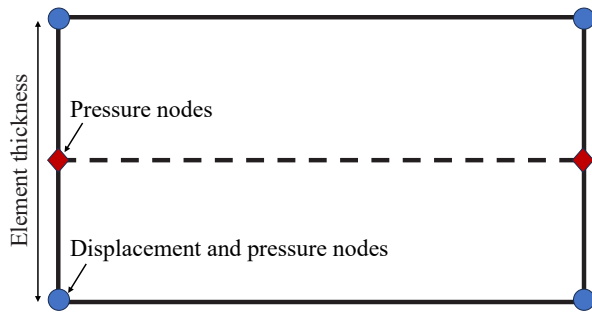


Fig. 3. Cohesive element with pore pressure nodes.

$$\frac{\partial w}{\partial t} - \nabla \left(\frac{w^3}{12\mu} \nabla p_f \right) + 2c(p_f - p_p) = q_{inj} \delta(x, y) \quad (7)$$

where t represents the time; q_{inj} represents the injection rate; and $\delta(x, y)$ represents the Dirac delta function. The temporary plugging area restricts tangential fluid flow. The flow of fluid in the temporary plugging area should conform to Darcy's law, such as Eq. (8). Therefore, by increasing the equivalent viscosity of the fluid, it becomes possible to simulate the flow resistance within the plugging area.

$$v = -\frac{k_p}{\mu} \nabla p \quad (8)$$

After combining Eqs. (8) and (5), the equivalent viscosity equation is expressed as:

$$\mu_m = \frac{w^3 \mu}{12Ak_p} \quad (9)$$

where μ_m represents the equivalent viscosity; A and k_p respectively represent the cross-sectional area and permeability of the temporary plugging body. Eq. (9) is the basis of the equivalent viscosity method (EVM), which assumes that the fracture width and temporary plugging area are constant and the permeability of the plugging area varies with the changes in equivalent viscosity. Therefore, modifying the equivalent viscosity is a practical method to simulate the temporary plugging behavior.

2.2 Global embedded cohesive elements

According to the cohesive damage theory, fracture propagation occurs due to material separation and breakage in the cohesive region at the fracture tip, overcoming the cohesive force. Two methods exist for describing the cohesive region within the finite element theoretical framework, namely, the additive method and the embedded method. The difference lies in the embedding of fracture elements into the initial elements (Alfano et al., 2009). Two techniques, the embedded method and the additive method, have the capability to model the process of generating and propagating hydraulic fractures. In the embedded method, the fracture elements are meshed between the integral elements. In contrast, in the additive method, fracture elements are introduced into the integral cells when the stresses reach the cohesive strength. The embedded method is typically favoured as cohesive elements are integrated into the finite element mesh, leaving the topological mesh connectivity intact. This allows for easy implementation

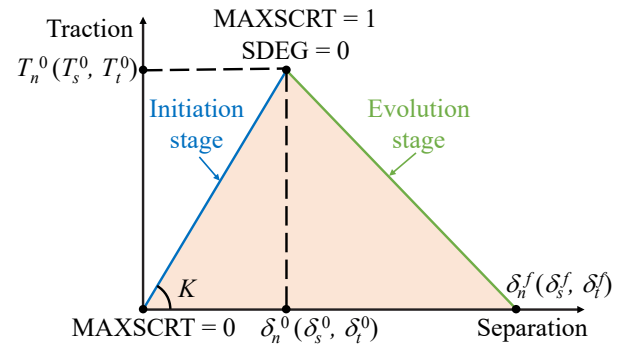


Fig. 4. Diagram of damage initiation and evolution pattern.

with regards to mesh and computational parallelisation, which is why the embedded model is employed in this article. To simulate the hydraulic fracturing process using an actual physical model mechanism, Segura and Carol (2008) developed the cohesive element with the pore pressure of zero-thickness (CEPPZ). This model employs a 6-node quadrilateral element that includes pore pressure nodes. Nodes 1 to 4, which surround the quadrilateral element, possess degrees of freedom for displacement and pore pressure. In contrast, nodes 5 and 6 are solely assigned pore pressure degrees of freedom (Fig. 3). A zero-thickness cohesive element is formed by considering the element thickness as zero.

The quadratic nominal stress criterion is employed to ascertain the occurrence of a fracture within CEPPZ. This criterion is formulated as:

$$\left\{ \frac{\langle T_n \rangle}{T_n^0} \right\}^2 + \left\{ \frac{T_s}{T_s^0} \right\}^2 + \left\{ \frac{T_t}{T_t^0} \right\}^2 = 1 \quad (10)$$

where T_n , T_s , and T_t represent the nominal traction forces applied in different directions of the CEPPZ; T_n^0 , T_s^0 and T_t^0 correspond to the nominal stress peaks in various orientations of the material, typically referring to the tensile and shear strengths. In 3D contexts, the subscripts n , s and t represent the normal direction perpendicular to the interface and the 1st and 2nd tangential directions on the interface, respectively. In 2D contexts, the 2nd tangential direction t is omitted. Fig. 4 shows the damage initiation and evolution law of CEPPZ, and the relationship between the variables is expressed as:

$$\begin{cases} G_{Ic} = \frac{1}{2} T^0 \delta^f \\ K = \frac{T^0}{\delta^0} \\ E = KH_{eff} \end{cases} \quad (11)$$

where T^0 and δ^0 represent the damage initiation stress and displacement; δ^f represents the damage failure displacement; G_{Ic} represents the normal fracture energy; K represents the stiffness; E represents the modulus; and H_{eff} represents the physical thickness. The damage initiation and evolution of CEPPZ are divided into two processes. The first one, known as the loss initiation stage, is characterized by an increase in the traction force as the separation displacement enlarges. The traction force reaches its peak value, that is, the loss initiation stress, when the separation displacement reaches the damage initiation level. This marks the onset of the second process,

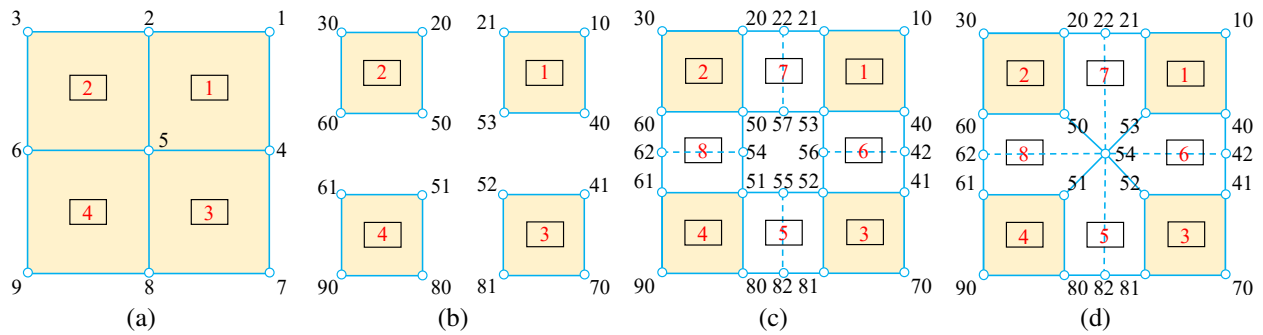


Fig. 5. Embedding CEPPZ method. (a) original cells; (b) reconstructing cells; (c) embedding CEPPZ; and (d) merging percolation nodes.

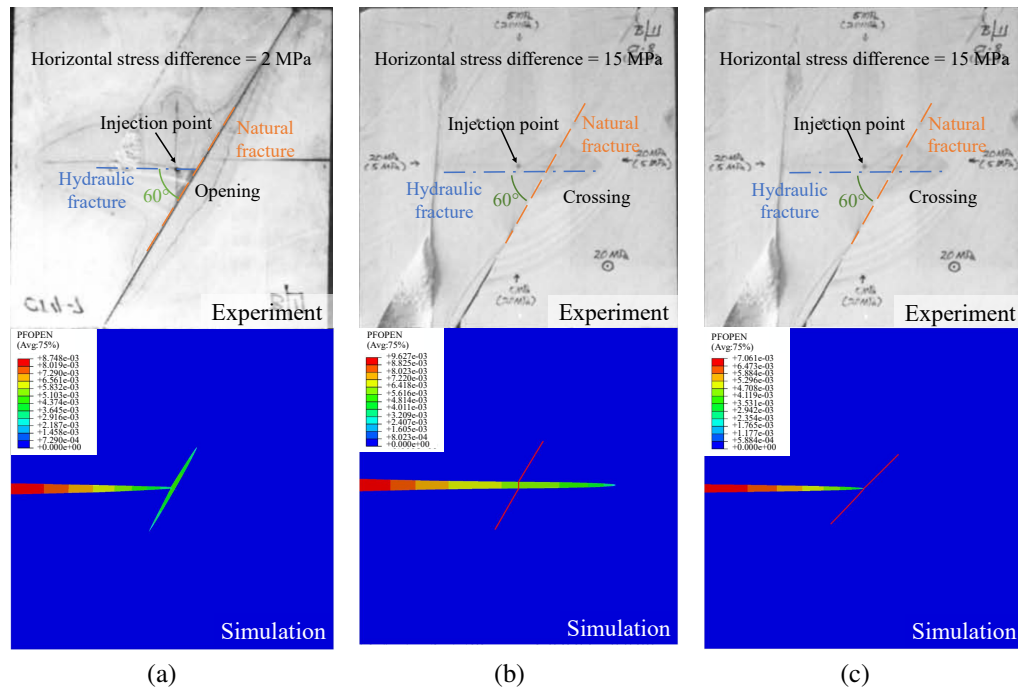


Fig. 6. Comparison of model and experimental results (Blanton, 1982). (a) 60° and 2 MPa; (b) 60° and 15 MPa; and (c) 45° and 15 MPa.

i.e., the damage evolution process. In this process, the traction force decreases with an increase in separation displacement until it eventually becomes zero, leading to the destruction of the element. In the first stage, the traction force and separation displacement are linearly related, with the slope determined by the stiffness. The modulus is the product of the stiffness and the physical thickness. When the work of traction force reaches the normal fracture energy, the cohesive unit is destroyed.

For the unimpeded propagation of HF, the CEPPZ is incorporated into the grid trajectory, using the component mesh framework as the foundational structure. The seepage nodes of adjacent elements are merged to ensure the fluid connection between adjacent CEPPZs. As shown in Fig. 5, in simple terms, based on the pre-divided grid, the common nodes are copied, the elements are decomposed and reconstructed, and the CEPPZ is embedded. Then, the adjacent seepage nodes are

merged. In addition, the thickness of CEPPZ is zero, which has been enlarged for clarity in the figure. Many nodes in the figure overlap in a physical location, such as nodes 50, 51, 52, 53, and 54.

3. Model validation

3.1 Interaction between NF and HF

Blanton (1982) studied the intersection problem of NF and HF via indoor experiments. His experimental results were used for comparison to validate the accuracy of our model (Fig. 6). The model results were consistent with the experimental results under different intersection angles (i.e., 45° and 60°) and HSD (i.e., 2 and 15 MPa). When the intersection angle was the same and the HSD was different, the interaction results between HF and NF were different, crossing or opening NF (Figs. 6(a) and 6(b)).

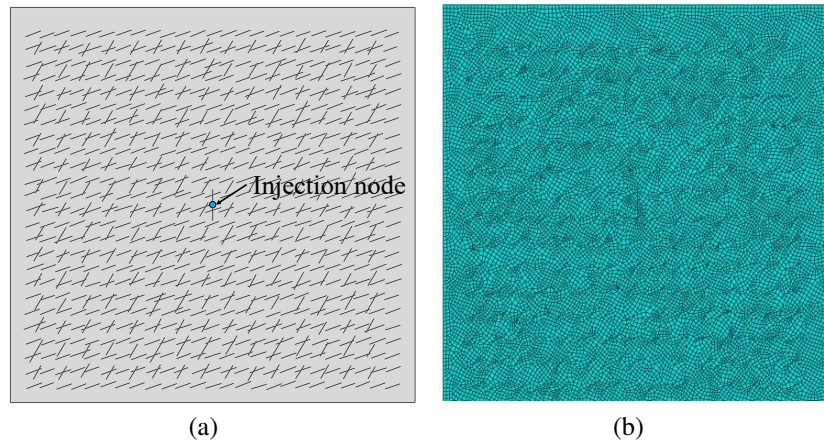


Fig. 7. In-seam FTPDF model. (a) NF distribution and (b) mesh.

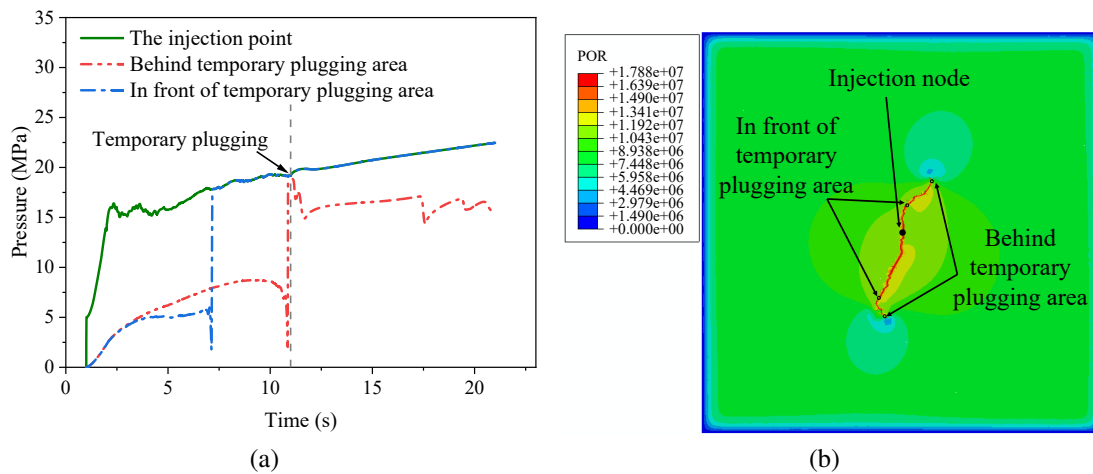


Fig. 8. Simulation results under temporary plugging. (a) pressure variation at different locations and (b) pore pressure diagram during fracturing.

3.2 Temporary plugging effect

A 2D FTPDF model for a fractured reservoir was established, and the NF distribution and the mesh were shown in Fig. 7. It was partitioned into 16,075 quadrilateral cells with four nodes (bilinear displacement, bilinear pore pressure), representing the rock matrix and assuming a size of $50 \text{ m} \times 50 \text{ m}$. To facilitate random fracture extension, 31,930 COH2D4P elements (the 4-node, 2D pore pressure cohesive element with transitional modeling from Darcy flow to Poiseuille flow) were embedded between the matrix elements using the global embedded CEPPZ method. The input parameters of the model were listed in Table 1. There were two sets of NF with different directions, and the length and direction of each fracture group followed normal distribution, while the position of NF followed uniform distribution (Fig. 7(a)). All subsequent studies were based on this parameter, with the parameter settings based on the experimental studies of Sierra et al. (2010) and the model settings of Gonzalez et al. (2015).

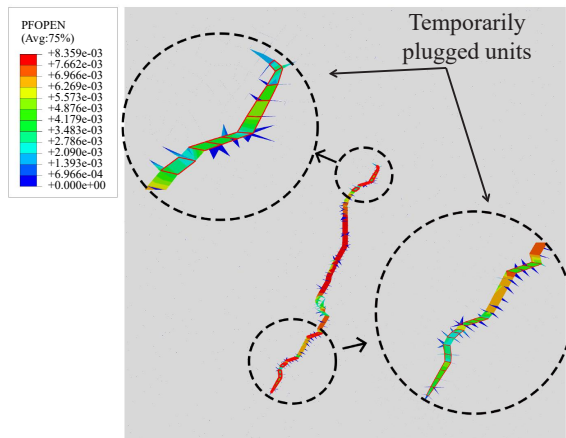
The FTPDF simulation consisted of three stages. Stage #1 involved injecting fluid at the injection point in the center

of the model to form a fracture. Stage #2 was the selection and implementation of temporary plugging elements. The fracture elements damaged in stage #1 were extracted, and screening was performed to identify elements that necessitated temporary plugging based on the extent of fracture opening. The EVM was employed, assigning properties to the plugged elements to augment the fluid viscosity. Stage #3 was the diverting fracturing process. Although the operation of this stage was similar to that of stage #1, the plugging elements resulted in the initiation of new fractures that were not opened during stage #1.

In order to ascertain the effectiveness of temporary plugging, the equivalent viscosity, fluid viscosity, plugging timing, and injection displacement were $10 \text{ Pa}\cdot\text{s}$, $1 \text{ mPa}\cdot\text{s}$, 11^{th} s , and $0.01 \text{ m}^2/\text{s}$, respectively. The pressure at three specific locations was monitored, as shown in Fig. 8(b). After the implementation of temporary plugging, a substantial decrease in pressure was observed at the location behind the plugging area (i.e., red line in Fig. 8(a)), establishing a significant disparity compared to the pressures recorded at the other two

Table 1. Basic parameters.

Object	Variable	Value
Rock matrix and NF	Stiffness (GPa/m)	15
	Fluid leak-off coefficient ($\text{m}^2/(\text{Pa}\cdot\text{s})$)	4.5×10^{-15}
	Poisson's ratio	0.2
	Permeability coefficient (m/s)	5×10^{-7}
	Initial void ratio (%)	10
Rock matrix	Tensile strength of joints (MPa)	6
	Fracture energy of joints (kPa-m)	3
	Intersection angles ($^\circ$)	30 or 70
	Average length (m)	2
NF	Line density of 30° NF (strips/m)	0.3
	Line density of 70° NF (strips/m)	0.5
	Tensile strength of joints (MPa)	2
	Fracture energy of joints (kPa-m)	1

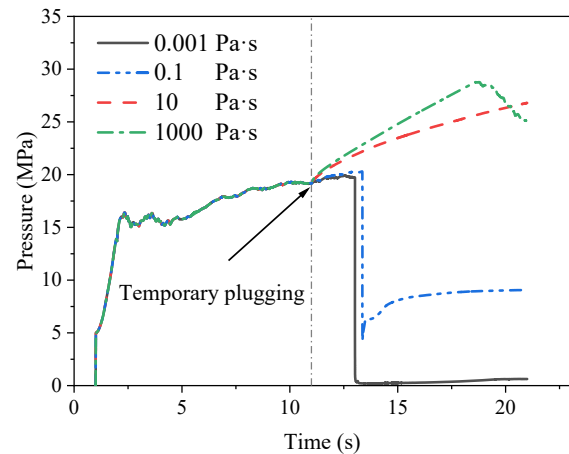
**Fig. 9.** Fracture morphology and plugging position.

points. These findings validated the efficacy of the temporary plugging simulation method. Before the temporary plugging, a sudden pressure drop occurred in two instances, followed by recovery, at distinct points away from the injection point. This phenomenon was caused by a sudden change in the crack aperture as the cohesive element at the crack tip separated during the extension process, creating a low-pressure vacuum zone. Fig. 8(b) depicts a localized low-pressure area at the apex of HF, which progressively extended outward as the fracture itself expanded.

4. Results and discussion

4.1 Impact of permeability of the plugging area

Diversified temporary plugging agents formed a plugging area with different permeabilities at the front of HF, and the plugging area permeability directly affected the effectiveness of FTPDF. The EVM was used to investigate the influence of plugging area permeability on FTPDF, and the fracture morph-

**Fig. 10.** Injection pressure curves.

ology and temporary plugging positions obtained from stages #1 and #2 of FTPDF were presented in Fig. 9. The fluid viscosity, plugging timing and injection displacement were 1 mPa·s, 11th s, and 0.015 m²/s, respectively. The simulation results were shown in Figs. 10 and 11. An increase in equivalent viscosity (i.e., a decrease in the plugging area permeability) after temporary plugging led to a more accelerated increase in fracture pressure (Fig. 10). When the equivalent viscosity reached 1,000 Pa·s, new fractures were successfully initiated, leading to a significant decrease in fracture pressure (Fig. 11(d)). In situations of low equivalent viscosity, the heterogeneity of the formation led to the initial expansion of the lower fracture, extending it to the model boundary and causing a sudden decrease in pressure (Figs. 11(a) and 11(b)). When the permeability and range of the plugging area were insufficient to induce fracture diversion during the corresponding injection rate, the temporary plugging impeded HF growth (Fig. 11(c)). Therefore, if the plugging area permeability was

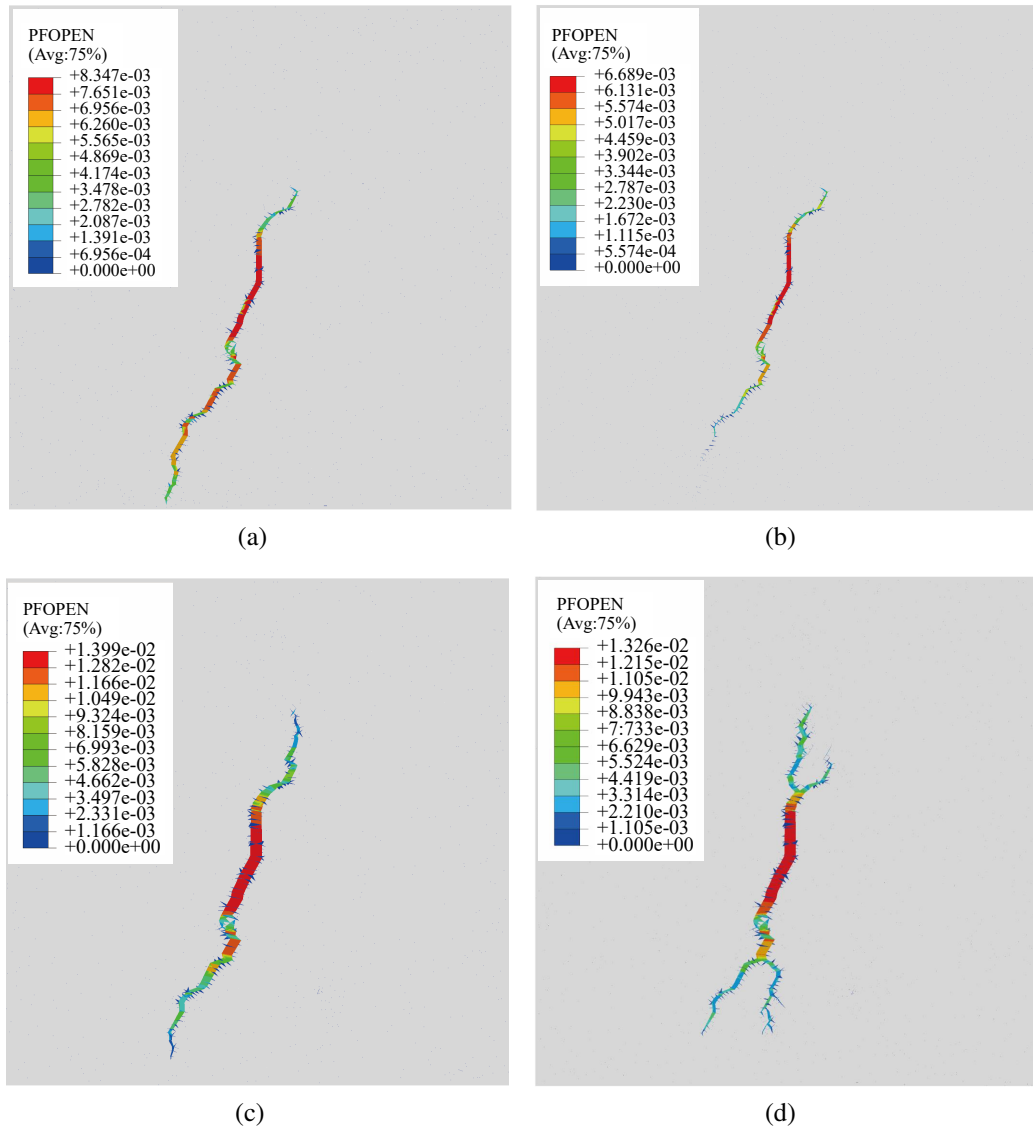


Fig. 11. Simulation results of fracture propagation under different equivalent viscosities. (a) 0.001 Pa·s; (b) 0.1 Pa·s; (c) 10 Pa·s; and (d) 1000 Pa·s.

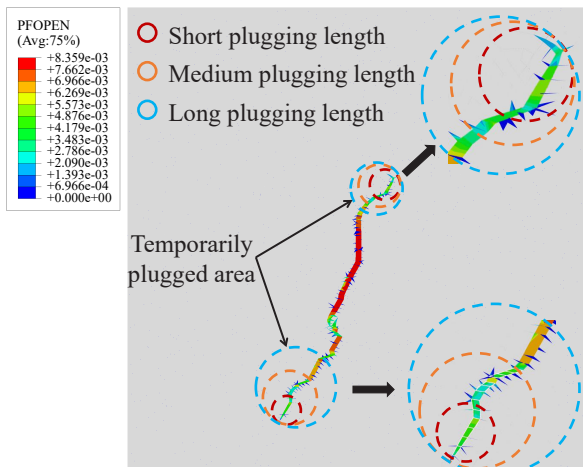


Fig. 12. Fracture morphology and plugging position.

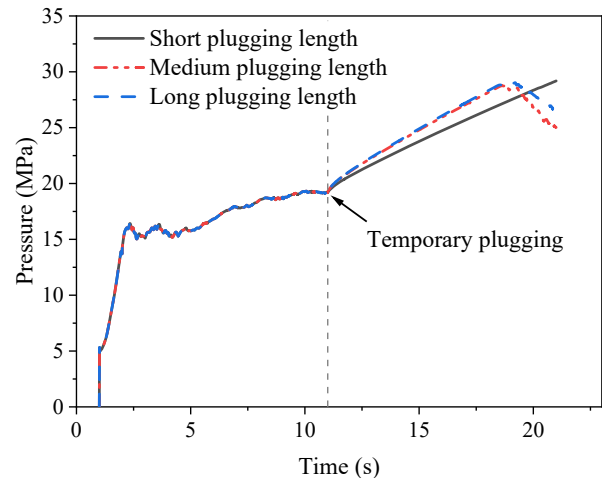


Fig. 13. The curves of injection pressure.

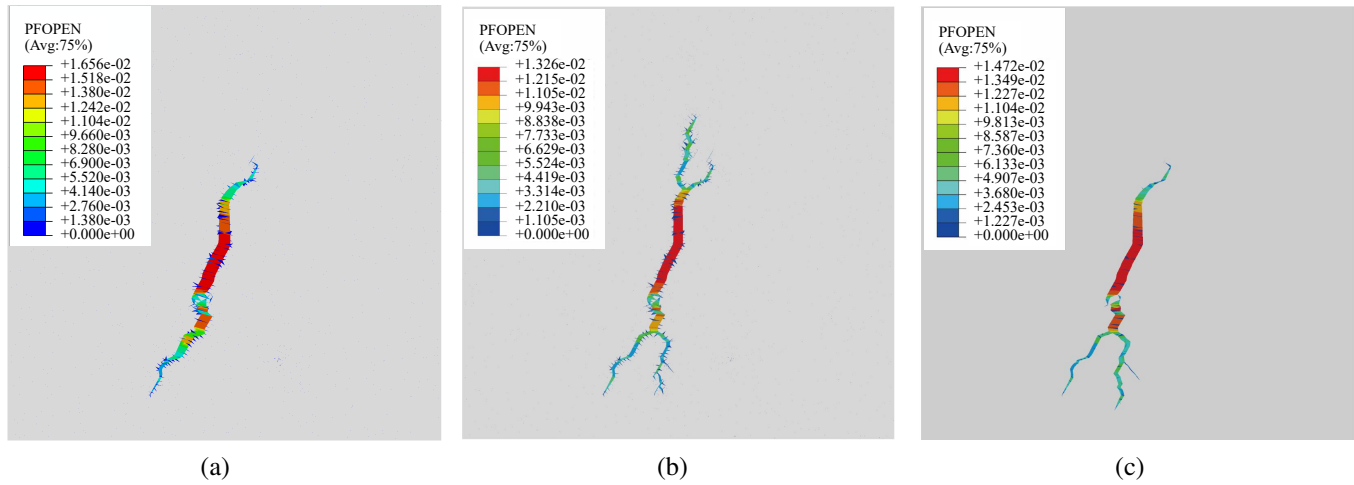


Fig. 14. Simulation results of fracture propagation under different plugging lengths. (a) short plugging length; (b) medium plugging length; and (c) long plugging length.

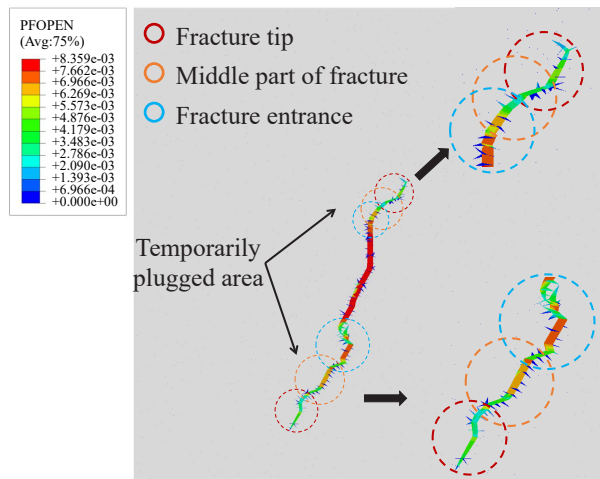


Fig. 15. Fracture morphology and plugging position.

too high, it was impossible to form effective temporary plugging and divert the fracture.

4.2 Impact of plugging area length

Different concentrations and dosages of temporary plugging agents led to the generation of plugging zones of varying lengths. By examining the width range of HF, different numbers of fracture elements were selected and temporarily blocked. This method was employed to investigate the effects of plugging area length on fracture propagation. The fracture elements with a width range of 3.5 to 4.5 mm were considered as short plugging length, 3.5 to 5.5 mm as medium plugging lengths, and 3.5 to 6.5 mm as long plugging lengths (Fig. 12). The equivalent viscosity, fluid viscosity, plugging timing, and injection displacement were 1,000 Pa·s, 1 mPa·s, 11th s, and 0.015 m²/s, respectively. The simulation results were shown in Figs. 13 and 14. These indicated that augmenting the plugging length had a positive impact on increasing the pressure within fractures (Fig. 13) and promoted the generation of new fractures (Fig. 14). Nevertheless, as the plugging length

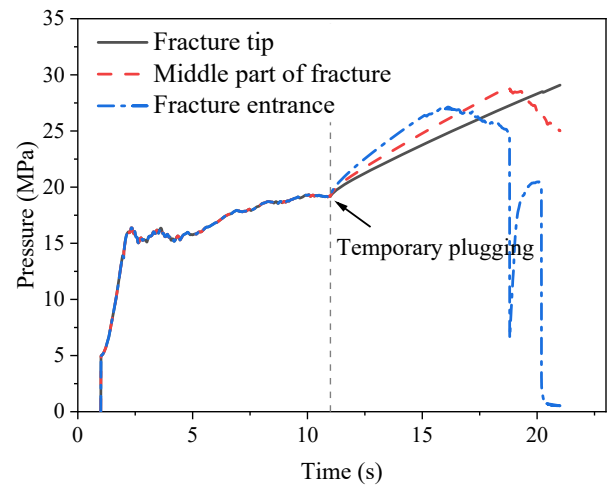


Fig. 16. Injection pressure curves.

reached a certain threshold, its influence on the increase in crack pressure diminished progressively (e.g., the red and blue lines in Fig. 13). Thus, it was unnecessary to increase the dosage of temporary plugging agents indiscriminately.

4.3 Impact of plugging position

Adjusting the type and grain size of the temporary plugging agents can enable temporary plugging at any point along the fracture. The fracture elements at different positions from the injection point were temporarily blocked (Fig. 15). The equivalent viscosity, fluid viscosity, plugging timing, and injection displacement were 1,000 Pa·s, 1 mPa·s, 11th s, and 0.015 m²/s, respectively, and the effects of plugging position on fracture propagation were investigated. The simulation results were shown in Figs. 16 and 17. The pressure within the fracture rose more quickly as the temporary plugging position neared the injection point (Fig. 16). The temporary plugging area too close or too far relative to the injection point could not yield the expected results (Figs. 17(a) and 17(c)). When the temporary plugging position was too close to the injection

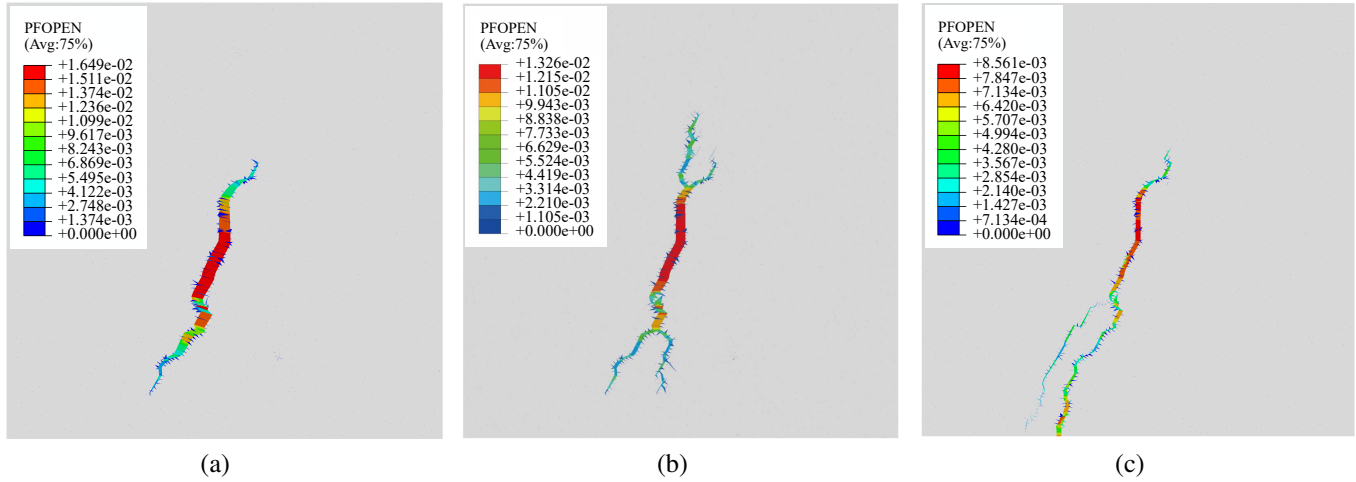
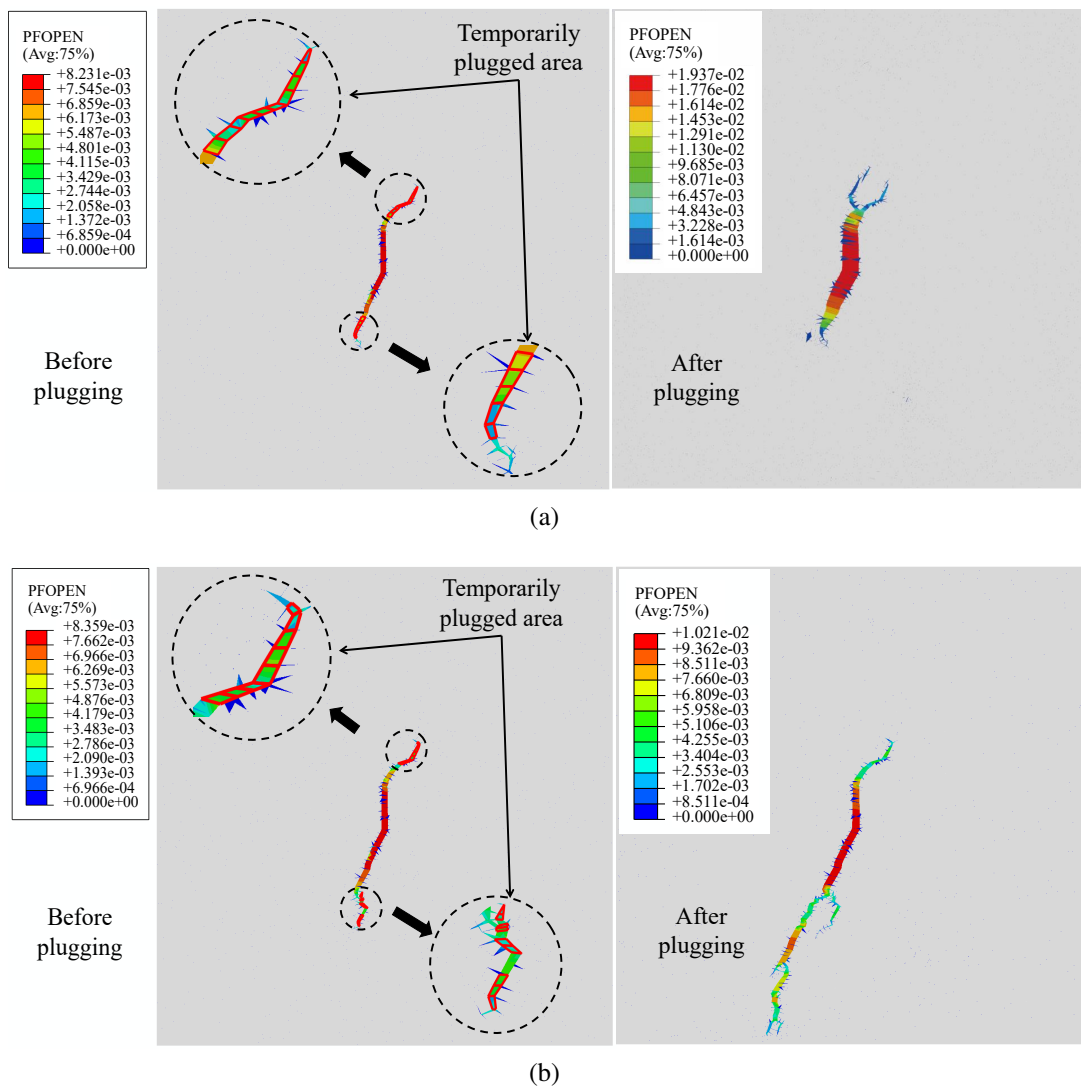


Fig. 17. Simulation results of fracture propagation under different plugging positions. (a) fracture entrance; (b) middle part of fracture; and (c) fracture tip.



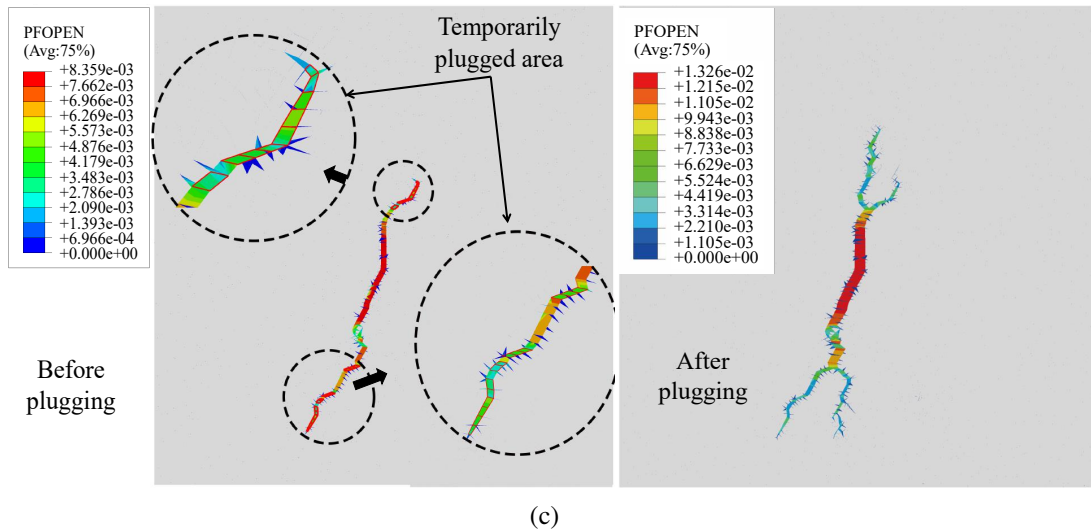


Fig. 18. Simulation results of fracture propagation under different plugging timings. (a) plugging at 6th s; (b) plugging at 8th s; and (c) plugging at the 11th s.

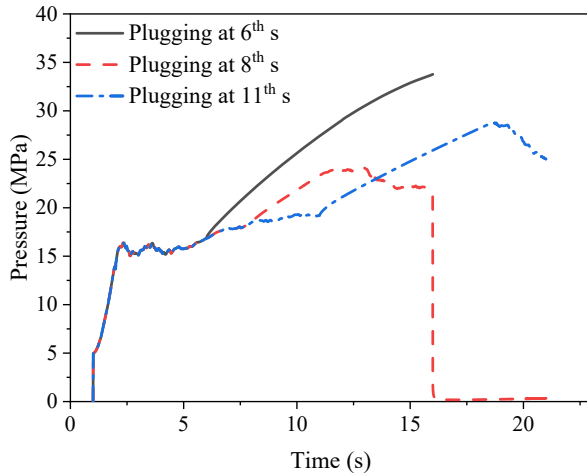


Fig. 19. Curves of injection pressure under different plugging timings.

point, there were fewer geological weak planes between the plugging position and the injection point.

4.4 Impact of plugging timing

During the practical FTPDF process, there were no specific guidelines on the timing or the duration of the injection of temporary plugging agents. The influence of the timing of temporary plugging on fracture expansion was examined by implementing plugging at different time intervals. The equivalent viscosity, fluid viscosity and injection displacement were 1,000 Pa·s, 1 mPa·s and 0.015 m²/s, respectively, and the fracture width range for temporary plugging was the same. The specific area was shown on the left side of Fig. 18. The simulation results were illustrated in Figs. 18 and 19. Early plugging led to a swift pressure increase that reached the maximum limit of the model (e.g., the black line in Fig. 19), which resulted in the opening of only one new fracture above the model in the plugging area, causing the

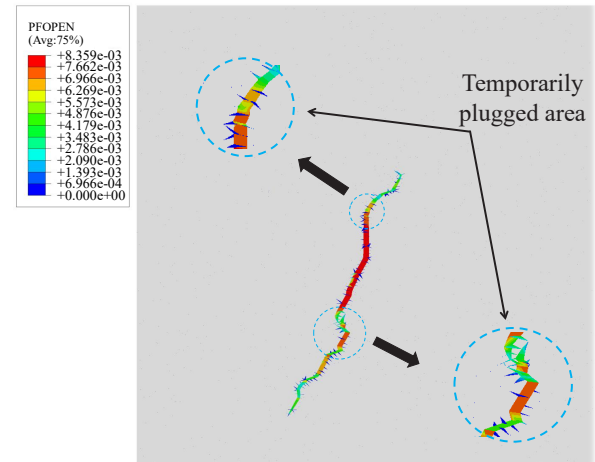


Fig. 20. Fracture morphology and plugging position.

pressure not to decrease. When comparing Figs. 18(a) and 18(b), appropriately delaying the timing of temporary plugging seems beneficial for forming a more complex fracture network.

4.5 Impact of displacement and viscosity

In traditional fracturing, injection displacement and fluid viscosity significantly influence fracture expansion. Thus, we investigated the impacts of these factors on FTPDF. The plugging positions remained consistent across all models, and the specific temporary plugging area was shown in Fig. 20. However, variations in fluid viscosity modified the equivalent viscosity at the plugging positions, maintaining the ratio of equivalent viscosity at 10⁴. The simulation results were presented in Figs. 21 and 22. The injection pressure slightly increased with the increase in fluid viscosity (Fig. 21), which was attributed to a decrease in fluid loss perpendicular to the fracture, resulting in more fluid retained within the fracture. Moreover, a rise in fluid viscosity impeded the expansion of HF by increasing the resistance to tangential flow and

enhancing the plugging effect in the temporary plugging zone. However, the latter had a more substantial impact than the former. A viscosity increase reduced the asymmetry of HF on both the upper and lower sides, causing the originally shorter upper fracture to extend and the longer lower fracture to shorten (Fig. 22). An increase in injection displacement had a more pronounced effect on the pressure within the fracture and the fracture width than viscosity, given the same proportion (Figs. 21 and 22).

5. Conclusion

This study used the finite element method with EVM and CEPPZ to establish a 2D FTPDF model in a fractured reservoir and discussed the effects of injection parameters and temporary plugging parameters on fracture propagation. Some interesting conclusions were drawn as follows:

- 1) Reducing the plugging area permeability resulted in a quicker pressure increase within the fracture, raising the probability of initiating a new fracture and achieving directional fracturing. To ensure the opening of new frac-

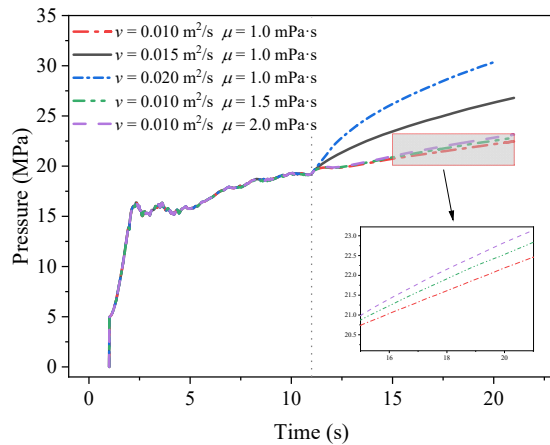


Fig. 21. Injection pressure curves.

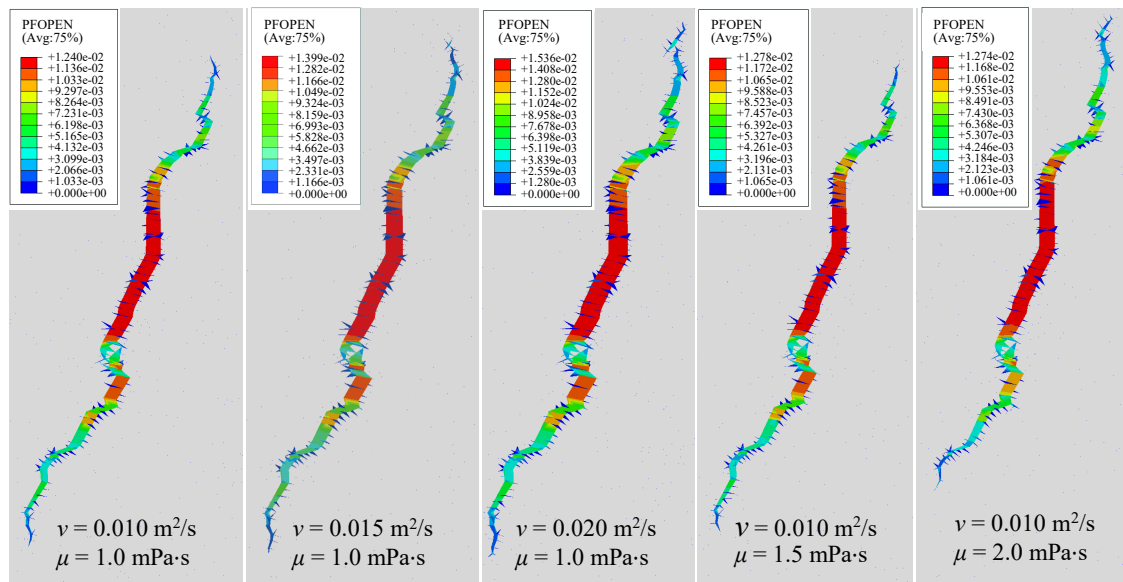


Fig. 22. Simulation results of fracture propagation under different injection displacements and fluid viscosities.

tures, the equivalent viscosity of the plugging area should be greater than 10 Pa·s.

- 2) Lengthening the plugging area significantly augmented the pressure rise within the fracture. However, once the length of plugging area reached a specific threshold, its impact on pressure elevation waned.
- 3) The choice of the plugging position should consider the density and distribution of NF. Ensuring adequate interaction between the plugging position, the initial HF, and the NF within the formation is crucial.
- 4) Temporary plugging should be conducted after elongating the initial HF to its maximum extent.
- 5) The increase in fluid viscosity and injection displacement elevated the injection pressure, and the effect of injection displacement was significantly greater than that of fluid viscosity.

Acknowledgements

This work was supported by the Science and Technology Cooperation Project of the CNPC-SWPU Innovation Alliance (No. 2020CX0105).

Conflict of interest

The authors declare no competing interest.

Open Access This article is distributed under the terms and conditions of the Creative Commons Attribution (CC BY-NC-ND) license, which permits unrestricted use, distribution, and reproduction in any medium, provided the original work is properly cited.

References

- Abdelaziz, A., Ha, J., Li, M., et al. Understanding hydraulic fracture mechanisms: From the laboratory to numerical modelling. *Advances in Geo-Energy Research*, 2023, 7(1): 66-68.
- Alfano, M., Furguiele, F., Leonardi, A., et al. Mode I fracture

- of adhesive joints using tailored cohesive zone models. *International Journal of Fracture*, 2009, 157: 193-204.
- Blanton, T. L. An experimental study of interaction between hydraulically induced and pre-existing fractures. Paper SPE 10847 presented at the SPE Unconventional Gas Recovery Symposium, Pittsburgh, Pennsylvania, 16-18 May, 1982.
- Chen, J., Zhang, Q., Zhang, J. Numerical simulations of temporary plugging-refracturing processes in a conglomerate reservoir under various in-situ stress difference conditions. *Frontiers in Physics*, 2022, 9: 826605.
- Chen, X., Zhao, L., Liu, P., et al. Experimental study and field verification of fracturing technique using a thermo-responsive diverting agent. *Journal of Natural Gas Science and Engineering*, 2021, 92: 103993.
- Clifton, R. J., Abou, A. S. A variational approach to the prediction of the three-dimensional geometry of hydraulic fractures. Paper presented at the SPE/DOE Low Permeability Gas Reservoirs Symposium, Denver, Colorado, 27-29 May, 1981.
- Geertsma, J., Haafkens, R. A comparison of the theories for predicting width and extent of vertical hydraulically induced fractures. *Journal of Energy Resources Technology*, 1979, 101(1): 8-19.
- Gonzalez, M., Taleghani, A. D., Olson, J. E. A cohesive model for modeling hydraulic fractures in naturally fractured formations. Paper SPE 173384 presented at the SPE Hydraulic Fracturing Technology Conference, The Woodlands, Texas, USA, 3-5 February, 2015.
- Hunt, G. E., Batchelor, G. K. An introduction to fluid dynamics. *The Mathematical Gazette*, 1968, 52(380): 206-207.
- Jiang, T., Bian, X. Multistage circuitous-temporary plugging fracturing technology for deep oil-gas reservoirs. *Journal of Shenzhen University Science and Engineering*, 2021, 38(6): 590-597. (in Chinese)
- Kresse, O., Weng, X., Wu, R., et al. Numerical modeling of hydraulic fractures interaction in complex naturally fractured formations. Paper ARMA 2012292 presented at the 46th U.S. Rock Mechanics/Geomechanics Symposium, Chicago, Illinois, 24-27 June, 2012.
- Li, J., Dong, S., Hua, W., et al. Numerical simulation of temporarily plugging staged fracturing based on cohesive zone method. *Computers and Geotechnics*, 2020, 121: 103453.
- Li, J., Yang, H., Qiao, Y., et al. Laboratory evaluations of fiber-based treatment for in-depth profile control. *Journal of Petroleum Science and Engineering*, 2018, 171: 271-288.
- Meyer, B. R., Bazan, L. W. A discrete fracture network model for hydraulically induced fractures-theory, parametric and case studies. Paper SPE 140514 presented at the SPE Hydraulic Fracturing Technology Conference, The Woodlands, Texas, USA, 24-26 January, 2011.
- Segura, J. M., Carol, I. Coupled HM analysis using zero-thickness interface elements with double nodes. Part I: Theoretical model. *International Journal for Numerical and Analytical Methods in Geomechanics*, 2008, 32(18): 2083-2101.
- Settari, A., Cleary, M. P. Development and testing of a pseudo-three-dimensional model of hydraulic fracture geometry. *SPE Production Engineering*, 1986, 1(6): 449-466.
- Sierra, R., Tran, M. H., Abousleiman, Y. N., et al. Woodford shale mechanical properties and the impacts of lithofacies. Paper ARMA 10461 presented at the 44th U.S. Rock Mechanics Symposium and 5th U.S.-Canada Rock Mechanics Symposium, Salt Lake City, Utah, 27-30 June, 2010.
- Wang, D., Dong, Y., Sun, D., et al. A three-dimensional numerical study of hydraulic fracturing with degradable diverting materials via CZM-based FEM. *Engineering Fracture Mechanics*, 2020a, 237: 107251.
- Wang, J., Xu, H., Yang, K., et al. Process simulation and performance evaluation of plugging cakes during temporary plugging and diverting fracturing. *Petroleum Science and Technology*, 2022a, 40(20): 2504-2524.
- Wang, X., Zhang, F., Yin, Z., et al. Numerical investigation of refracturing with/without temporarily plugging diverters in tight reservoirs. *Petroleum Science*, 2022b, 19(5): 2210-2226.
- Wang, W., Zheng, D., Sheng, G., et al. A review of stimulated reservoir volume characterization for multiple fractured horizontal well in unconventional reservoirs. *Advances in Geo-Energy Research*, 2017, 1(1): 54-63.
- Wang, B., Zhou, F., Wang, D., et al. Numerical simulation on near-wellbore temporary plugging and diverting during re-fracturing using XFEM-based CZM. *Journal of Natural Gas Science and Engineering*, 2018, 55: 368-381.
- Wang, B., Zhou, F., Yang, C., et al. Experimental study on injection pressure response and fracture geometry during temporary plugging and diverting fracturing. *SPE Journal*, 2020b, 25(2): 573-586.
- Weng, X., Kresse, O., Cohen, C., et al. Modeling of hydraulic-fracture-network propagation in a naturally fractured formation. *SPE Production & Operations*, 2011, 26(4): 368-380.
- Wu, K., Olson, J. E. Simultaneous multifracture treatments: Fully coupled fluid flow and fracture mechanics for horizontal wells. *SPE Journal*, 2015, 20(2): 337-346.
- Wu, M., Wang, W., Song, Z., et al. Exploring the influence of heterogeneity on hydraulic fracturing based on the combined finite-discrete method. *Engineering Fracture Mechanics*, 2021, 252: 107835.
- Yu, H., Taleghani, A. D., Lian, Z. On how pumping hesitations may improve complexity of hydraulic fractures, a simulation study. *Fuel*, 2019, 249: 294-308.
- Zhang, F., Damjanac, B., Maxwell, S. Investigating hydraulic fracturing complexity in naturally fractured rock masses using fully coupled multiscale numerical modeling. *Rock Mechanics and Rock Engineering*, 2019, 52(12): 5137-5160.
- Zhao, L., Chen, X., Zou, H., et al. A review of diverting agents for reservoir stimulation. *Journal of Petroleum Science and Engineering*, 2020, 187: 106734.
- Zhou, H., Wu, X., Song, Z., et al. A review on mechanism and adaptive materials of temporary plugging agent for chemical diverting fracturing. *Journal of Petroleum Science and Engineering*, 2022, 212: 110256.